# CHAPTER IV
# RESULTS AND DISCUSSION

According to the previous work, Kritsanakun *et al.*, (2013) studied the effect of metal loading in bi-functional catalysts (Pt/HY) for the hydrotreated renewable jet (HRJ) fuel production from hydrogenated biodiesel (HBD) derived from jatropha oil. From the catalytic activity testing results, the 0.1 wt% Pt/HY showed a high jet fuel yield with 3 times lower metal loading as compared to 0.3 wt% Pt/HY. Consequently, 0.1 wt% Pt loading was chosen to be a catalyst in this research.

## 4.1 Feed and Standard Analysis

The chromatogram of various *n*-paraffin feedstocks in the hydrogenated biodiesel range including pentadecane (*n*-$C_{15}$), hexadecane (*n*-$C_{16}$), heptadecane (*n*-$C_{17}$) and octadecane (*n*-$C_{18}$) analyzed by a GC/FID (Agilent 7890A) which equipped with DB-5 column is shown in Figure 4.1. Besides peaks of the *n*-paraffins, a little amount of *iso*-paraffins was also observed. Moreover, the peak of carbon disulfide used as a solvent appeared on the chromatogram at 1.20 min.

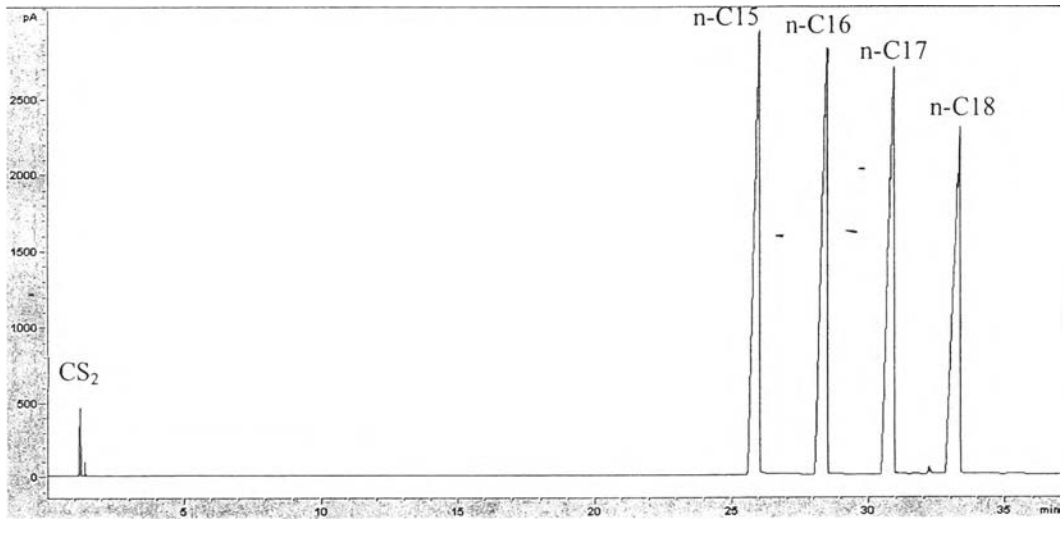


**Figure 4.1** Chromatogram of various *n*-paraffin feedstocks in the HBD range analyzed by a GC/FID.

In order to identify the products, it is necessary to determine the retention times for each products peak by using mixture of standard chemicals. The chromatogram of standard chemicals for potential products is shown in Figure 4.2 while the retention times for the standard chemicals are listed in Table 4.1.

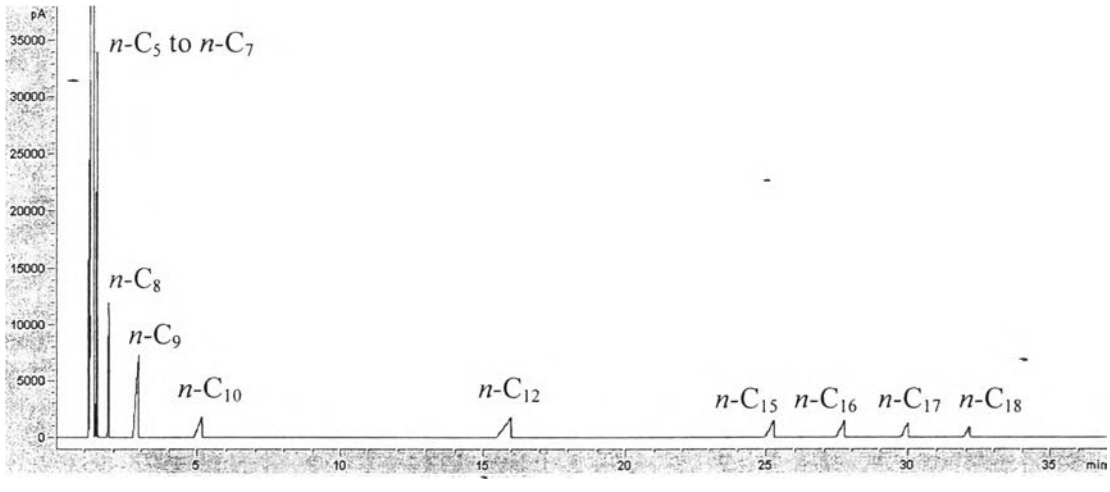


**Figure 4.2** Chromatograms of standard chemicals including *n*-pentane (*n*-$C_5$), *n*-hexane (*n*-$C_6$), *n*-heptane (*n*-$C_7$), *n*-octane (*n*-$C_8$), *n*-nonane (*n*-$C_9$), *n*-decane (*n*-$C_{10}$), *n*-dodecane (*n*-$C_{12}$), *n*-pentadecane (*n*-$C_{15}$), *n*-hexadecane (*n*-$C_{16}$), *n*-heptadecane (*n*-$C_{17}$), *n*-octadecane (*n*-$C_{18}$) analyzed by a GC/FID.

For the gas reference standard, it was analyzed by a GC/FID (Shimadzu GC-17A) equipped with HP-PLOT-$Al_2O_3$ column. The chromatogram of standard gas mixture is shown in Figure 4.3 and the retention times of the standard gas mixture are also listed in Table 4.1.

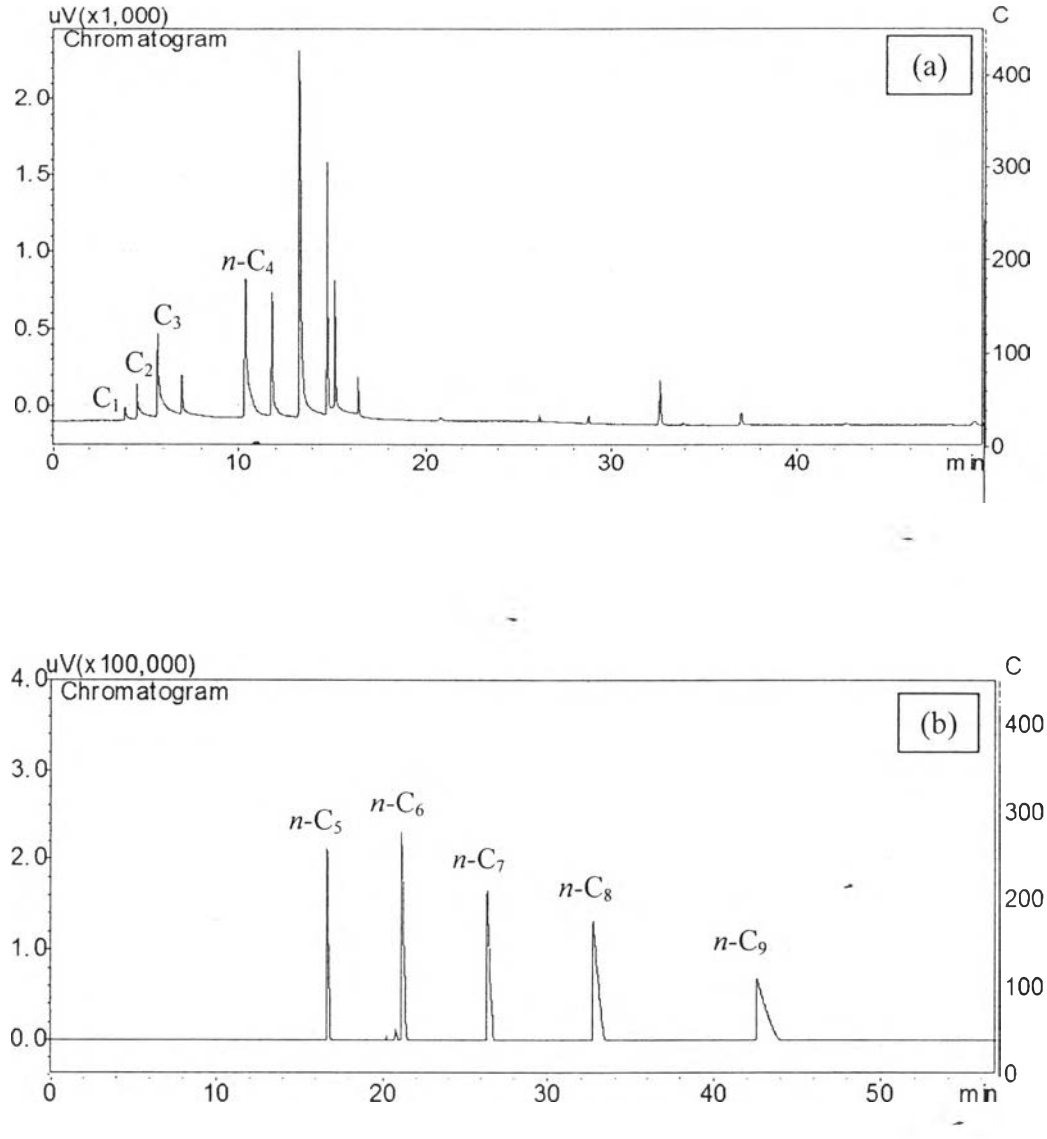


**Figure 4.3** Chromatogram of the standard gases, (a) methane, ethane, propane and *n*-butane, (b) *n*-pentane, *n*-hexane, *n*-heptane, *n*-octane and *n*-nonane.

**Table 4.1** Retention times of standard chemicals and standard gas mixture analyzed by a GC/FID (Agilent GC 7890A and Shimadzu GC-17A, respectively)

| Standard chemicals | Retention time | Standard gas mixture | Retention time |
|---|---|---|---|
| *n*-Pentane (*n*-$C_5$) | 1.14 | Methane ($C_1$) | 3.92 |
| *n*-Hexane (*n*-$C_6$) | 1.26 | Ethane ($C_2$) | 4.56 |
| *n*-Heptane (*n*-$C_7$) | 1.44 | Propane ($C_3$) | 6.96 |
| *n*-Octane (*n*-$C_8$) | 1.89 | *n*-Butane (*n*-$C_4$) | 11.80 |
| *n*-Nonane (*n*-$C_9$) | 2.95 | *n*-Pentane (*n*-$C_5$) | 15.95 |
| *n*-Decane (*n*-$C_{10}$) | 5.46 | *n*-Hexane (*n*-$C_6$) | 20.32 |
| *n*-Undecane (*n*-$C_{11}$) | 11.19 | *n*-Heptane (*n*-$C_7$) | 26.13 |
| *n*-Dodecane (*n*-$C_{12}$) | 16.26 | *n*-Octane (*n*-$C_8$) | 32.30 |
| *n*-Tridecane (*n*-$C_{13}$) | 19.97 | *n*-Nonane (*n*-$C_9$) | 41.73 |
| *n*-Tetradecane (*n*-$C_{14}$) | 22.96 | | |
| *n*-Pentadecane (*n*-$C_{15}$) | 25.95 | | |
| *n*-Hexadecane (*n*-$C_{16}$) | 28.39 | | |
| *n*-Heptadecane (*n*-$C_{17}$) | 30.76 | | |
| *n*-Octadecane (*n*-$C_{18}$) | 33.52 | | |

For example, a chromatograms of liquid and gas products obtained over Pt/HY (Si/Al ratio of 100) operated at operating conditions: 310 °C, 500 psig, LHSV of 1.0 $h^{-1}$, $H_2$/feed molar ratio of 30, and TOS of 6 h are shown in Figure 4.4. In Figure 4.4 (a), the chromatogram of liquid products was grouped into three main parts which are gasoline fuel ($C_5$-$C_8$), jet fuel ($C_9$-$C_{14}$), and remaining feed or diesel fuel ($C_{15}$-$C_{18}$) at the retention times of 1.14-2.95 min, 5.46-22.96 min, and 25.95-33.52 min, respectively. In Figure 4.4 (b), the chromatogram of gas products consisted of light fuel ($C_1$-$C_4$) and gasoline fuel ($C_5$-$C_8$) at the retention times of 3.92-11.80 min and 15.95-32.30, respectively.

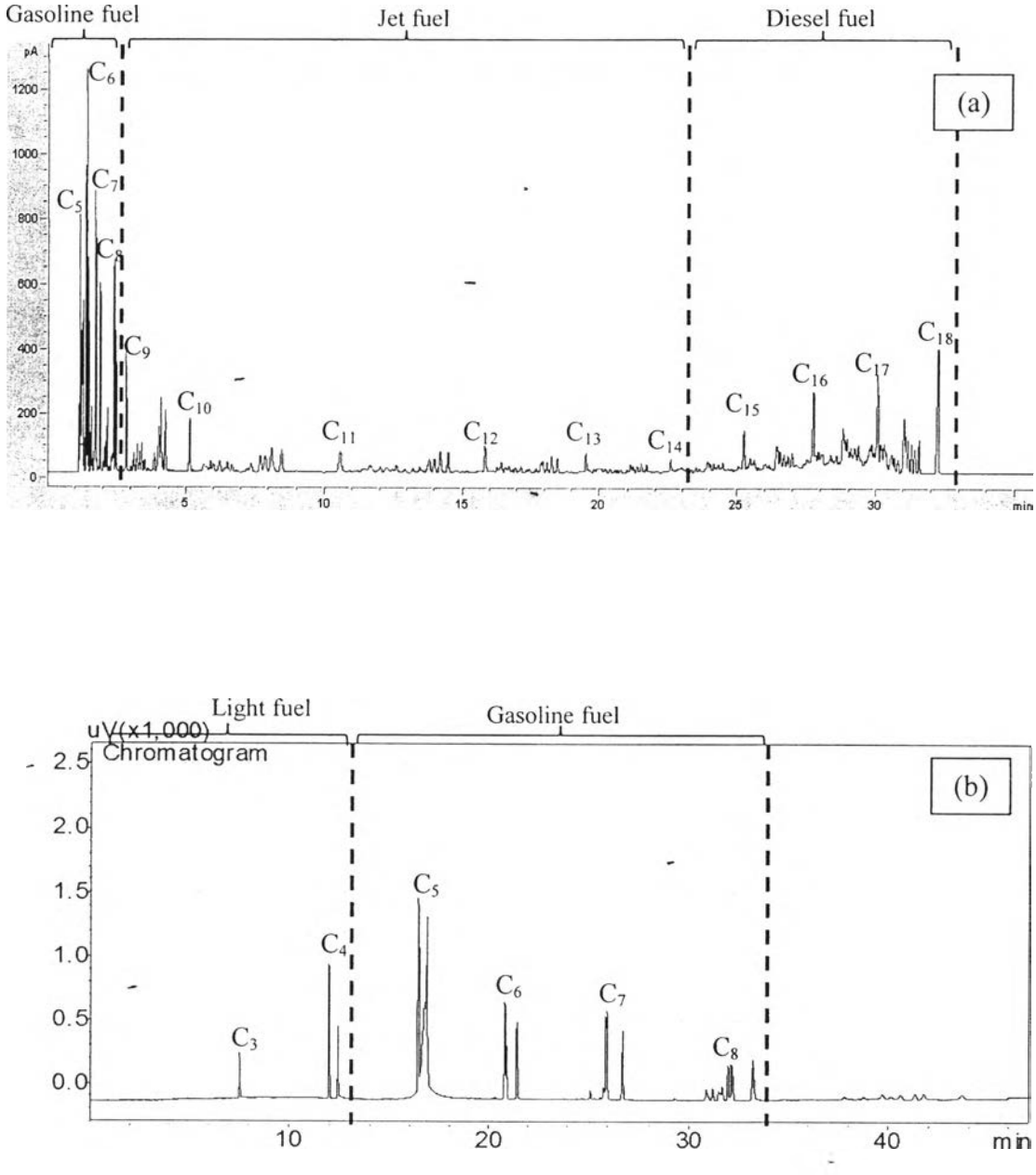


**Figure 4.4** Typical chromatogram of (a) liquid products and (b) gas products over Pt/HY (Si/Al ratio of 100) operated at operating conditions: 310 °C, 500 psig, LHSV of 1.0 $h^{-1}$, $H_2$/feed molar ratio of 30, and TOS of 6 h.

## 4.2 Characterization of Fresh Catalysts

### 4.2.1 Atomic Absorption Spectroscopy (AAS)

The actual metal loadings of the Pt supported HY catalysts prepared by different methods (IWI and IE) were determined by atomic absorption spectroscopy (AAS) technique. The AAS results are summarized in Table 4.2. The results revealed that the amounts of Pt on the HY support prepared by ion-exchange method compared with incipient wetness impregnation method were slightly different. The result confirmed that the Pt contents incorporated in HY zeolite were similar to the expected amount.

**Table 4.2** The desired Pt composition of the catalysts analyzed by AAS

| Catalyst | Actual Pt content (wt%) |
|---|---|
| 0.1 wt% Pt/HY (IWI) | 0.091 |
| 0.1 wt% Pt/HY (IE) | 0.093 |

### 4.2.2 Hydrogen Chemisorption

The reduced catalysts were characterized by hydrogen chemisorption to determine the dispersion of Pt on the catalysts. The dispersion was calculated from the amount of $H_2$ adsorbed on the Pt surface, assuming the H:Pt stoichiometry to be unity. The results are shown in Table 4.3. The hydrogen uptake (H/Pt) values obtained on the Pt/HY catalysts prepared by IWI and IE were 0.26 and 0.52, respectively. That is, the IE catalyst exhibited higher $H_2$ uptake than the IWI catalyst, indicating higher Pt dispersion. The uniform dispersion of metal zeolite catalyst prepared by IE and large Pt aggregation with poor dispersion of catalyst prepared by IWI were also observed by Li and Hsing (2006).

**Table 4.3** Hydrogen chemisorption of the prepared catalysts

| Catalyst | H/M (mol/mol) |
|---|---|
| 0.1 wt% Pt/HY (IWI) | 0.26 |
| 0.1 wt% Pt/HY (IE) | 0.52 |

4.2.3 Brunauer-Emmett-Teller (BET) Method

The textural properties of the different catalysts (surface area, total pore volume, and mean pore diameter) were obtained from the Brunauer–Emmett–Teller surface area analyzer as shown in Table 4.4. After impregnation and ion-exchange of catalyst, it showed the decrease in surface areas and pore volume as compared to the parent HY catalysts. This is owing to the metal filling into supported catalyst that could plug the pore of the support. Considering the catalyst prepared by different techniques, the surface area of the Pt/HY catalyst prepared by IWI and IE were slightly different because the actual presence of metal on IWI catalyst is a little less than that on IE catalyst as shown in AAS result.

**Table 4.4** Physical characteristics of the prepared catalysts

| Catalyst | BET surface area ($m^2/g$) | Pore volume* ($cm^3/g$) |
|---|---|---|
| HY | 654 | 0.54 |
| 0.1 wt% Pt/HY (IWI) | 642 | 0.53 |
| 0.1 wt% Pt/HY (IE) | 636 | 0.52 |

*using NLDFT method

4.2.4 Temperature Programmed Desorption (TPD) of Isopropylamine

The TPD of isopropylymine was used to quantify the Brønsted acid sites that catalyze the conversion of the isopropylamine into propylene and ammonia (Pereira and Gorte, 1992). The acidity of parent HY catalyst and 0.1 wt% Pt/HY catalyst prepared by IWI and IE techniques are summarized in Table 4.5. It was

found that the Brønsted acid density decreased with metal loading (Pt/HY) as compared to the parent catalyst. The decrease in Brønsted acid density could be due to the deposit of Pt on the acid sites of the zeolite. However, the total Brønsted acid sites of both catalysts, prepared by IWI and IE were slightly different with higher value of IWI catalyst. This could be due to the step of ion-exchange method resulting in the replacement of $H^+$ by $[Pt(NH_3)_4]^{2+}$.

**Table 4.5** Acidity of the HY parent (Si/Al 100) and Pt/HY prepared by IWI and IE method from TPD of isopropylamine

| Catalyst | Acidity of catalyst (μmol/g) |
|---|---|
| | **Brønsted site** |
| HY | 85.41 |
| 0.1 wt% Pt/HY (IWI) | 72.01 |
| 0.1 wt% Pt/HY (IE) | 68.29 |

4.2.5 Temperature Programmed Reduction (TPR)

In order to determine the reduction behavior of the catalysts, temperature programmed reduction was used to evaluate the reduction temperature of the investigated catalysts. The TPR profiles of 0.1 wt% Pt/HY catalysts prepared by different method (IWI and IE) after calcination up to 350 °C and HY support are shown in Figure 4.5. TPR spectrum of the parent HY support was also measured, which was a Pt free sample, this spectrum sufficiently illustrates the absence of any significant features in the temperature region below 300°C. The reduction profile of both catalysts which prepared by different methods display a major reduction peak at 110 °C merged with a minor peak near 200 °C and a broad peak near 400 °C. From some report (Ostgard *et al.*, 1992; Park *et al.*, 1986), it can indicate that the reduction peak at 110 °C is assigned to the reduction of $Pt^{2+}$ ions and $Pt^{4+}$ for the reduction peak at 400 °C. However, in this work, the catalyst precursor is a $Pt^{2+}$ salt $[Pt(NH_3)_4Cl_2]$; if autoreduction occurs under calcination conditions and the resulting $Pt^0$ atoms are oxidized, one would have to assume that $PtO_2$ is formed to account for

a Pt valence of 4+. This oxide could subsequently react with surface protons to generate water and Pt ions. The area under the peaks at 110 °C is larger in (c) than in (b) indicating a higher consumption of hydrogen than needed for the reduction of all $Pt^{2+}$ species to $Pt^0$. Considering the peak position, all peaks in (c) slightly shifted to higher temperature as compared to (b). This could be described that the catalysts prepared by IE method have a stronger interaction between metal and acidic support than IWI catalysts.

However, it was found that the broad peak near 400 °C of IWI catalyst was slightly larger than that of IE catalyst. This could be due to higher amount of $NH_4^+$ residue from precursor over IWI catalyst which led to autoreduction on the catalysts. For IE method, the catalysts were washed with DI water to remove the excess ions after ion-exchange step whereas the metal precursor solution in IWI method was impregnated on support without elimination of excess ions.

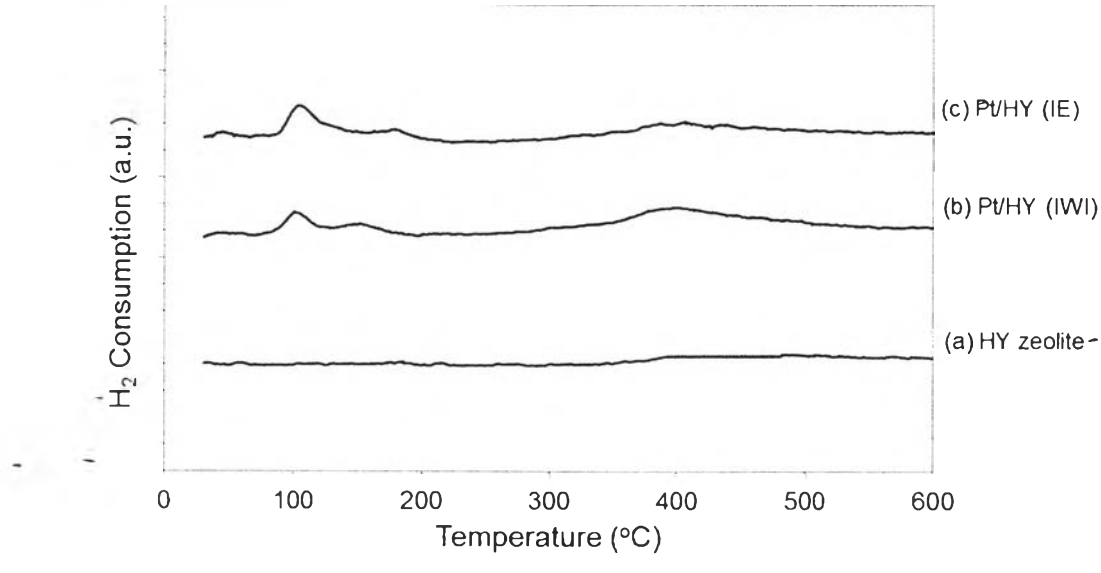


**Figure 4.5** Temperature programmed reduction (TPR) profiles of the HY zeolite and Pt/HY catalysts (a) HY zeolite, (b) Pt/HY prepared by IWI and (c) Pt/HY prepared by IE.

## 4.3 Catalytic Activity Testing

For studying of the catalytic activity, the conversion, product yield and selectivity of hydrocracking of various *n*-paraffin feedstocks ($C_{15}$-$C_{18}$) over the bi-functional catalysts, Pt/HY (Si/Al of 100) catalysts with 0.1 wt% Pt prepared by incipient wetness impregnation (IWI) and ion-exchanged techniques (IE) were investigated. The reaction conditions for hydrocracking of *n*-paraffin hydrocarbons were conducted at 310 °C, 500 psig, liquid hourly space velocity (LHSV) of 1.0 $h^{-1}$, and $H_2$/feed molar ratio of 30.

### 4.3.1 Effect of *n*-Paraffin Feedstock Chain Length

A distribution of cracked products both liquid and gas products analyzed by GC/FID (Agilent GC 7890A and Shimadzu GC-17A, respectively) is presented in term of selectivity, which were calculated with formulas as shown in Chapter III. Product selectivity of hydrocracking various *n*-paraffin feedstocks ($C_{15}$-$C_{18}$) obtained over Pt/HY catalysts prepared by IWI are shown in Figure 4.6 (in moles of product per mole converted feedstock). The carbon number distribution of cracked product showed virtually no $C_1$, $C_2$ and the hydrocarbons that would be obtained by splitting off $C_1$ and $C_2$ from the feed paraffin. In 1975, Weitkamp said that "In each case the curves are symmetrical indicating pure primary cracking. Methane and ethane as well as $C_{m-1}$ and $C_{m-2}$ (m represent the carbon number of feedstock) are virtually absent. Product distributions like this are typical for ideal hydrocracking." This absent phenomenon may result from mechanistic background. Branched carbenium ions are formed via *n*-alkenes and linear carbenium ions. Then, either desorption or $\beta$-scission may occur in parallel reactions. The cracking step occurs at the beta position because the C-C bond beta to the charged carbon on the carbenium ions is the weakest bond of the entire hydrocarbon chain and the easiest to break. This mechanism support that hardly any $C_1$ and $C_2$ hydrocarbons are formed.

Considering the shape of product distribution on Figures 4.6, the cracked product distribution exhibited the highest peak at carbon number 8 for all feedstock chain lengths ($C_{15}$ – $C_{18}$). For the *n*-$C_{17}$ and *n*-$C_{18}$ feedstocks, the results slightly deviated from the bell-shaped distribution curve of ideal hydrocracking

which the highest peak should be the center of carbon product distribution. This might be due to the structure of Y zeolite which has large pore diameter of 12 member oxygen ring at 7.4 Å and leads to a supercage of 13 Å in diameter. Table 4.6 summarizes the molecular length of various *n*-paraffin chain lengths presented by Gorring in 1973. It could illustrate that after the feedstock molecules enter into the pore of zeolite, as a complicated pore structure with 3-dimentional channel system. The long chain molecule limited transportation in the pore channel. Therefore, the long chain molecules were cracked into the shorter chain molecules. While the $C_8$ hydrocarbons, which has the molecular length of 12.82 Å and slightly smaller than the supercage size of Y zeolite (~13 Å), were the selective products for Y zeolite. This is the reason why the highest peak of cracked product distribution for the *n*-$C_{17}$ and *n*-$C_{18}$ feedstocks was hydrocarbon with 8 carbon atoms. Meanwhile, the distributions for the iso- and the normal-paraffin products of all feedstock chain lengths, the selectivity of *n*-paraffin products larger than $C_9$ remarkably decreased. This result could be described by the supercage size of Y zeolite and the molecular length of *n*-$C_9$. Because the molecular length of *n*-paraffin since carbon number 9 is larger than the supercage size of Y zeolite. Therefore, the most product of carbon number more than 9 was *iso*-paraffin product.

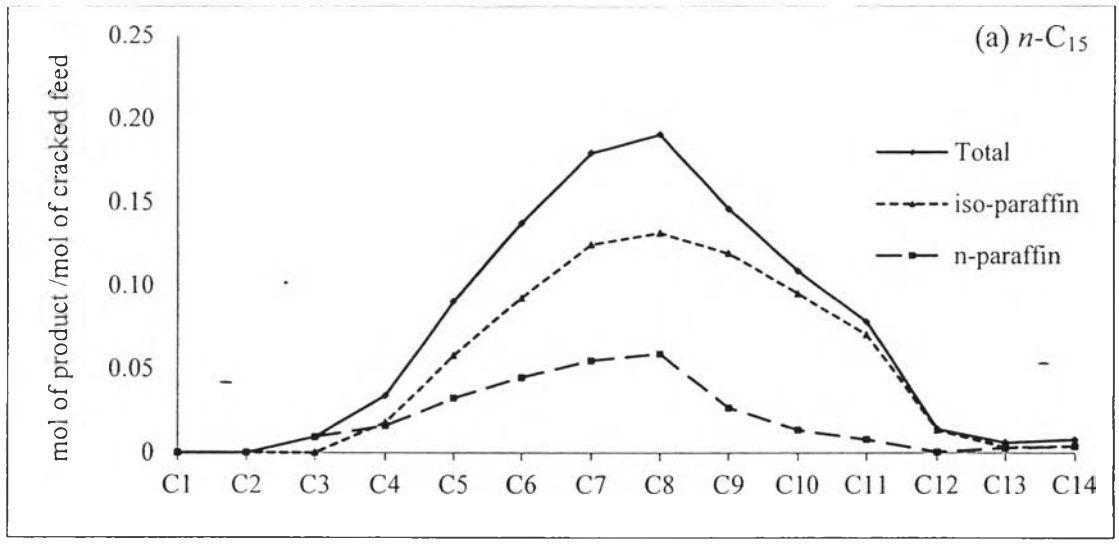


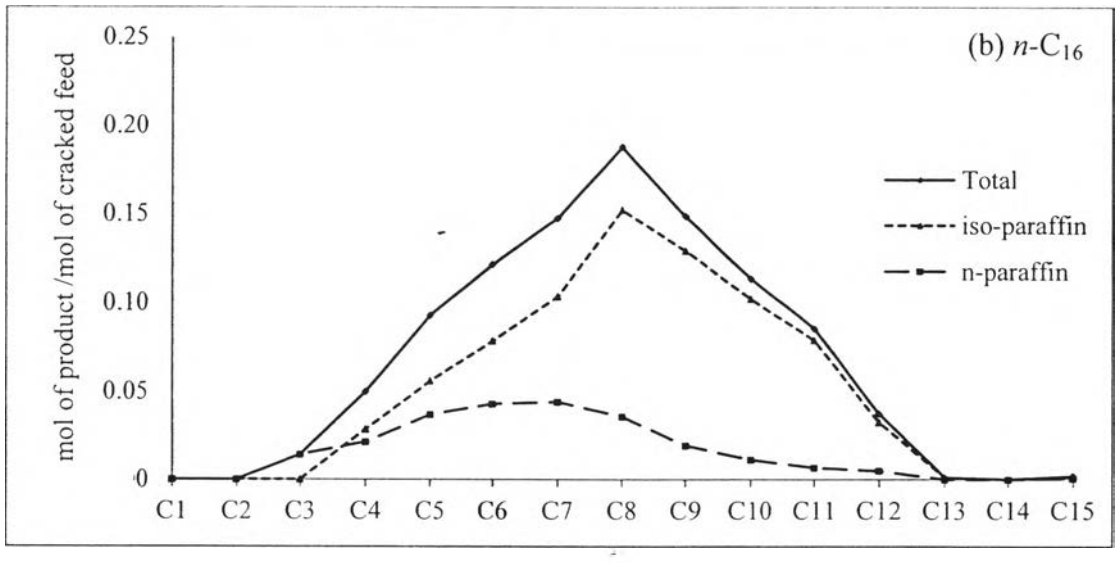


**Figure 4.6** Product distribution in cracking products (in moles of product per mole converted feedstock) over Pt/HY of various *n*-paraffin feedstocks; (a) *n*-pentadecane (*n*-$C_{15}$), (b) *n*-hexadecane (*n*-$C_{16}$), (c) *n*-heptadecane (*n*-$C_{17}$), and (d) *n*-octadecane (*n*-$C_{18}$) at operating condition: 310 °C, 500 psig, LHSV of 1.0 $h^{-1}$, $H_2$/feed molar ratio of 30, and TOS of 6 h.

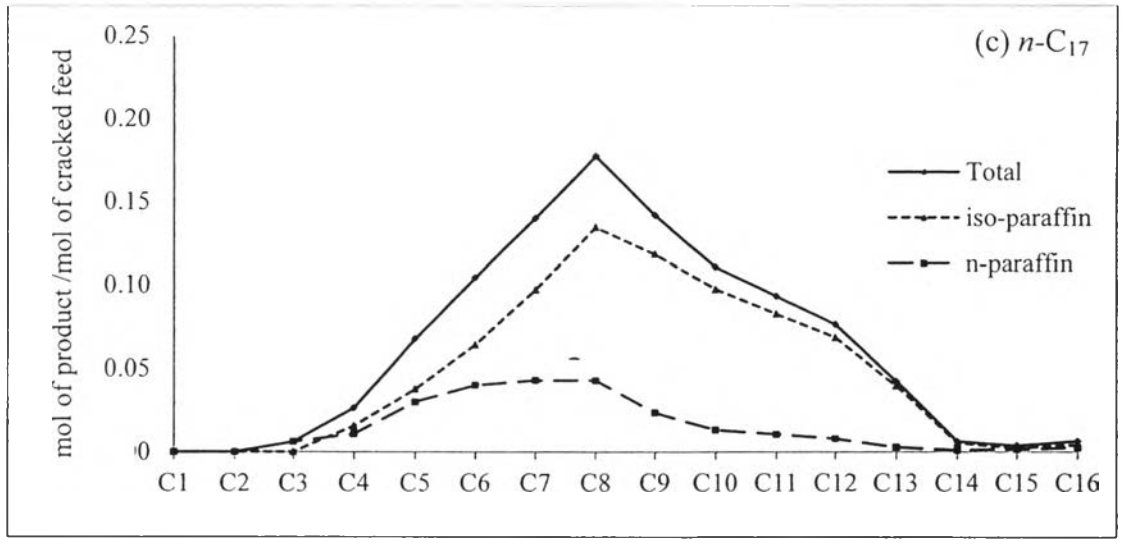


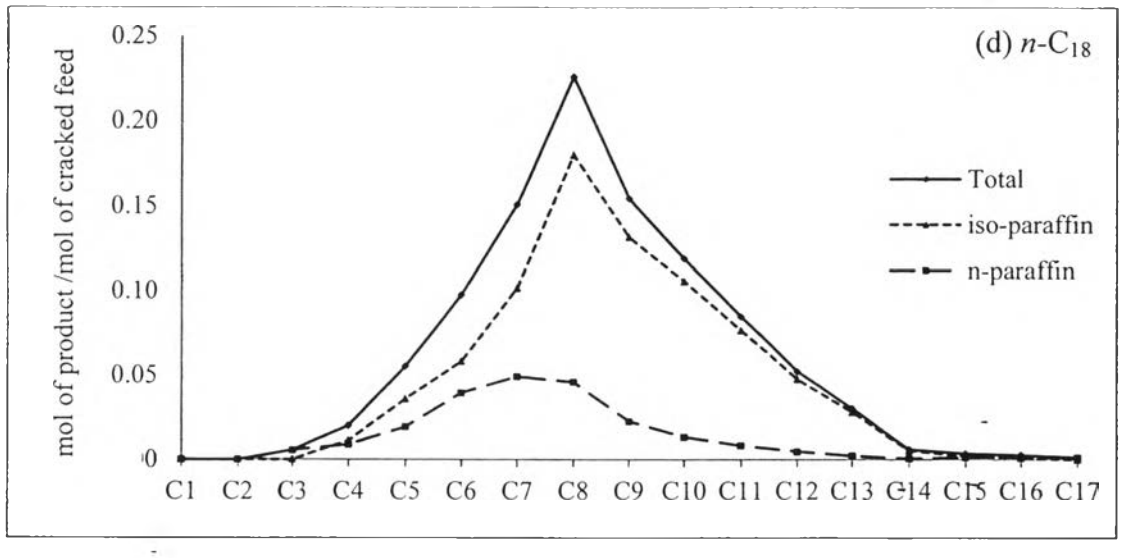


**Figure 4.6 (Cont.)** Product distribution in cracking products (in moles of product per mole converted feedstock) over Pt/HY of various *n*-paraffin feedstocks; (a) *n*-pentadecane (*n*-$C_{15}$), (b) *n*-hexadecane (*n*-$C_{16}$), (c) *n*-heptadecane (*n*-$C_{17}$), and (d) *n*-octadecane (*n*-$C_{18}$) at operating condition: 310 °C, 500 psig, LHSV of 1.0 $h^{-1}$, $H_2$/feed molar ratio of 30, and TOS of 6 h.

**Table 4.6** Molecular length of various *n*-paraffin chain lengths (Gorring, 1973)

| ***n*-Paraffin** | **Molecular length (Å)** |
|---|---|
| $C_1$ | 4.00 |
| $C_2$ | 5.26 |
| $C_3$ | 6.52 |
| $C_4$ | 7.78 |
| $C_5$ | 9.04 |
| $C_6$ | 10.30 |
| $C_7$ | 11.56 |
| $C_8$ | 12.82 |
| $C_9$ | 14.08 |
| $C_{10}$ | 15.34 |

Figure 4.7 shows the effect of the feed chain length on the product yield and total conversion of hydrocracking of different *n*-paraffin feedstocks over the IWI catalyst at the same operating condition. As shown in Figure 4.7, when feed chain length increased, the total conversion increased. This might be due to the effect of chain length on the crackability as reported by Voge in 1958, the very strong effect of chain length on the crackability of normal paraffins in the range from $C_5$ to $C_{24}$ has been observed. Assuming that all secondary carbon atoms ($-CH_2-$) of the straight paraffin have an equal chance of becoming the charge center of a secondary carbenium ion, one should expect the reactivities to be proportional to the total number of carbon atoms minus 2 (end of chain, $-CH_3$). Thus, reactivity of paraffins increased because of the increase in the available reaction pathways resulting in higher conversion.

In 1981, Steijns and Froment studied the effect of binary alkane mixtures on activity which found that the reactivities of individual compounds in mixtures might deviate from their behavior as single components. For example, in the conversion of an equimolar mixture of *n*-heptane and *n*-decane on Pt/US-Y. The conversion of the heavy *n*-alkane in the mixture was not affected by the presence of

the lighter compound. But the conversion of the light *n*-alkane was reduced compared to an individual feed under the same reaction conditions. These phenomena have been ascribed to competitive physisorption in the zeolite micropores (Steijns, M. and Froment, G., 1981). From assuming that reaction takes place after a molecule is adsorbed in the micropore system. Therefore, for a multicomponent system, if one component of feed is adsorbed preferentially, its concentration in the zeolite pore system will be higher than that of the other compounds. Hence this component could be converted more efficiently or prevent other compounds from being transformed (Denayer and Baron, 1997).

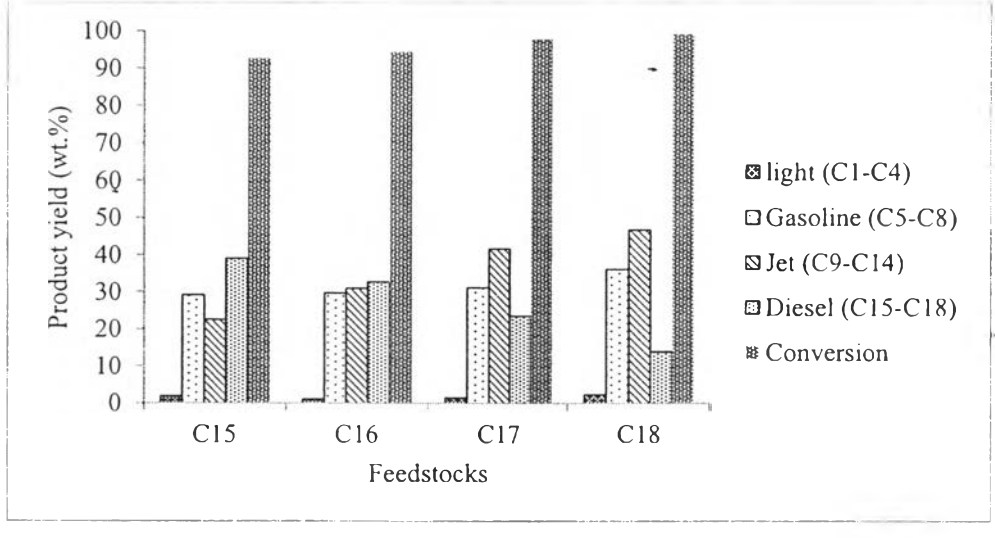


**Figure 4.7** Product yield and conversion of hydrocracking of various *n*-paraffin feedstocks over Pt/HY prepared by incipient wetness impregnation at operating condition: 310 °C, 500 psig, LHSV of 1.0 $h^{-1}$, $H_2$/feed molar ratio of 30, and TOS of 6 h.

Moreover, in 1997, Denayer and Baron also studied the effect of chain length and branching of paraffins (from $C_6$ to $C_{12}$) on adsorption and diffusion in zeolites. The result showed that the Henry constants of the paraffins increased exponentially with the chain length and the heats of adsorption also increased with molecular weight. The multicomponent adsorption can be reasonably well described by an extended Langmuir adsorption isotherm, in which the stronger adsorption of

the longer chains is reflected by their higher Henry constants. It could be concluded that longer chains are adsorbed preferentially over shorter chains.

4.3.2 Effect of Different Catalyst Preparation Methods

Selectivity of hydrocracking of individual *n*-paraffin feedstock (hexadecane, *n*-$C_{16}$) obtained on the Pt/HY catalysts prepared by different methods, IWI and IE, are shown in Figure 4.8. The results showed insignificant difference in carbon number product distribution pattern of hydrocracking of the same *n*-paraffin feedstock over different catalyst preparation methods. Thus it might be concluded that the catalyst preparation method did not create the notable difference on structure of the catalysts.

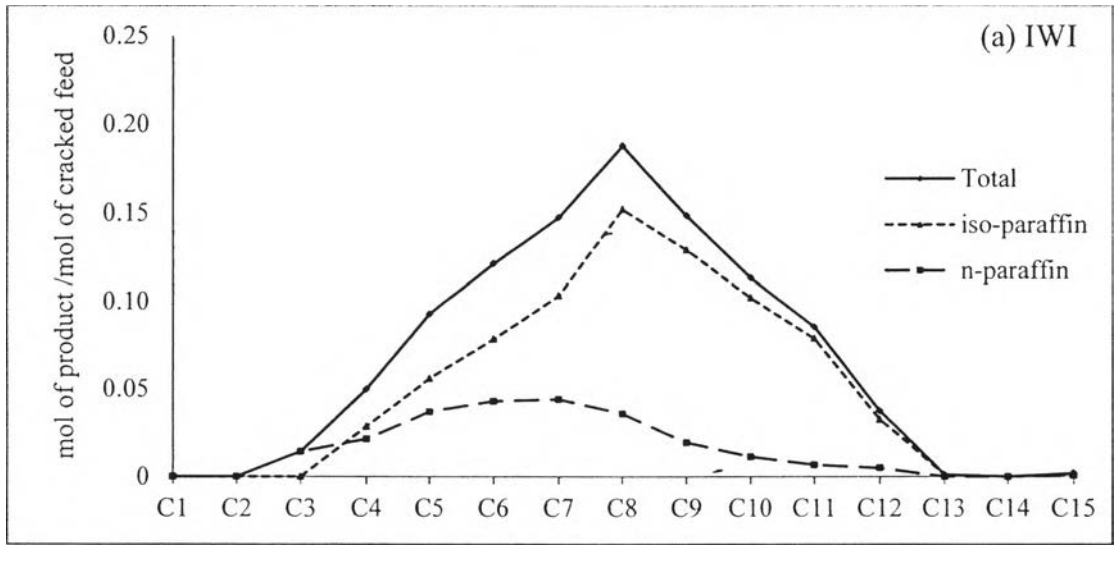


**Figure 4.8** Product distribution in cracking products (in moles of product per mole converted feedstock) of hexadecane ($C_{16}$) feedstock over Pt/HY prepared by (a) IWI, and (b) IE at operating condition: 310 °C, 500 psig, LHSV of 1.0 $h^{-1}$, $H_2$/feed molar ratio of 30, and TOS of 6 h.

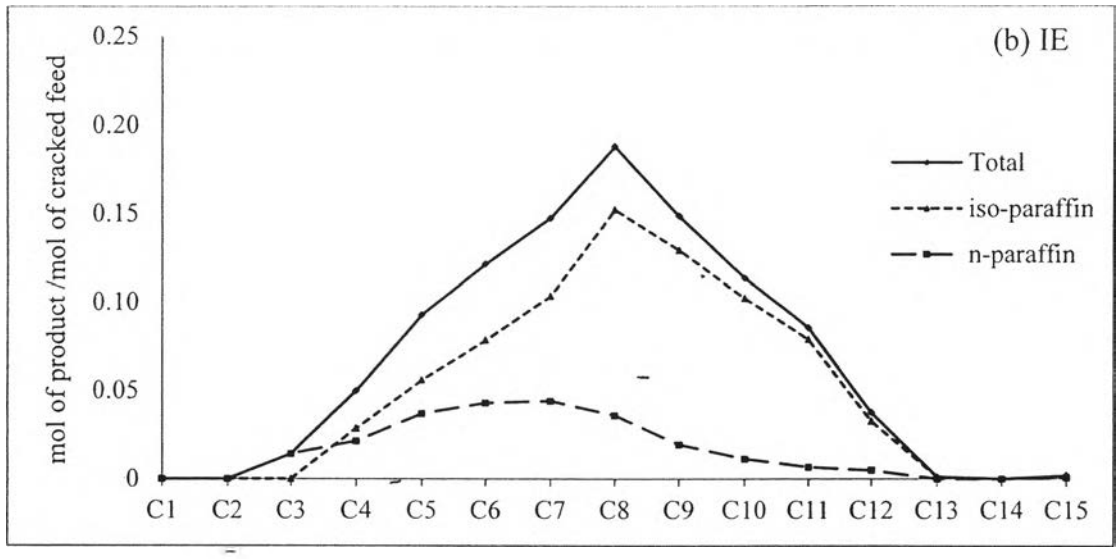


**Figure 4.8 (Cont.)** Product distribution in cracking products (in moles of product per mole converted feedstock) of hexadecane ($C_{16}$) feedstock over Pt/HY prepared by (a) IWI, and (b) IE at operating condition: 310 °C, 500 psig, LHSV of 1.0 $h^{-1}$, $H_2$/feed molar ratio of 30, and TOS of 6 h.

Figure 4.9 shows the effect of catalyst preparation technique on the product yield and total conversion of hydrocracking of the same *n*-paraffin feedstocks (hexadecane, *n*-$C_{16}$) on the Pt/HY prepared by different techniques, IWI and IE. The results showed that total conversion and light product yield (gasoline and jet fuels) over IE catalyst were higher than those observed over IWI catalysts. This result might be due to the dispersion of Pt resulting in an increasing the activities of the bi-functional catalysts, as observed from gasoline and jet product yield were increased while diesel yield was decreased. Likewise, on the classical hydrocracking mechanism over bi-functional catalyst (Denayer *et al.*, 1997), adsorbed alkanes are firstly dehydrogenated on the platinum metal clusters. Before the alkenes formed are protonated on the Brønsted acid sites and transformed into alkylcarbenium ions, the branched or cracked alkylcarbenium ions are deprotonated to rearranged alkenes, which are in turn hydrogenated to final products. Consequently, the metal clusters dispersion is one of the most essential factors to help the bifunctional mechanism occur promptly.

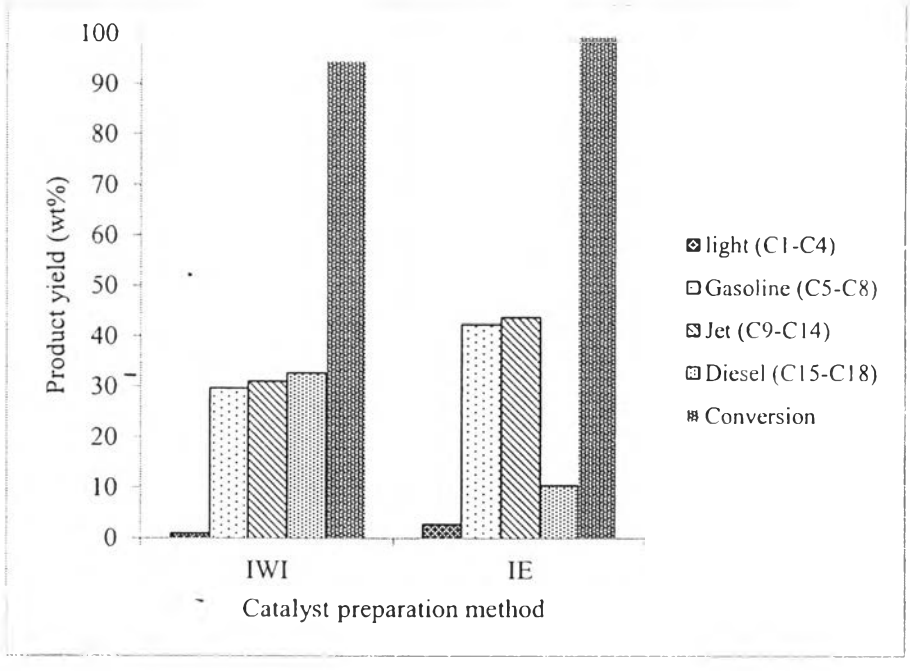


**Figure 4.9** Product yield and conversion of hydrocracking of hexadecane ($n$-$C_{16}$) feedstock over Pt/HY prepared by different method at operating condition: 310 °C, 500 psig, LHSV of 1.0 $h^{-1}$, $H_2$/feed molar ratio of 30, and TOS of 6 h.

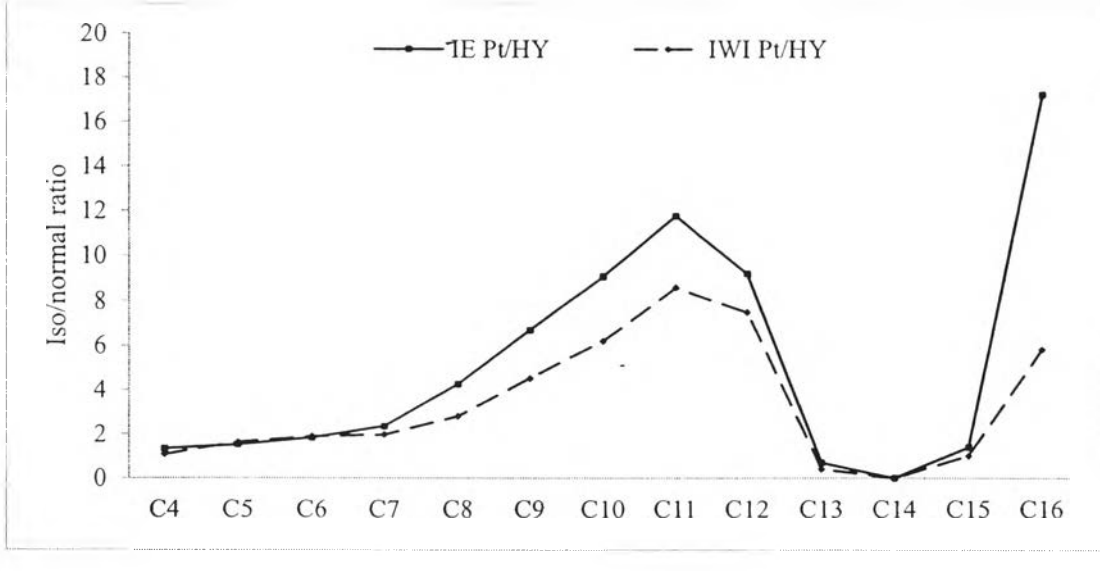


**Figure 4.10** Iso/normal ratio of cracked product obtained from hydrocracking of hexadecane ($n$-$C_{16}$) feedstock over Pt/HY prepared by different method at operating condition: 310 °C, 500 psig, LHSV of 1.0 $h^{-1}$, $H_2$/feed molar ratio of 30, and TOS of 6 h.

Figure 4.10 shows the fraction of branched products to straight-chain products from the hydrocracking reaction of $n$-$C_{16}$ on the Pt/HY prepared by different methods. On both of the catalysts, the fact that the ratio of iso/normal products exceeds 0.9 for main cracked products means that most of the cracked products obtained from hydrocracking reaction was branched products. This could indicate that the alkene formed by the metal sites must undergo isomerization before hydrocracking and followed by hydrogenation. Considering the different catalyst preparations, the iso/normal ratios of IE catalysts was higher than those observed on IWI catalysts for both of the main cracked products and the isomerized product. This could be hypothesized that the IE catalysts have isomerized activity higher than the IWI catalysts. This hypothesis leads to further study in transformation of $n$-paraffin feedstock on the Pt/HY catalyst prepared by different techniques.

Further study in details, the reaction pathways of $n$-alkane hydroisomerization and hydrocracking were determined with different catalyst preparation. As previously discussed, the different catalyst preparations caused the different amounts of metal dispersion which relate to the balance between the acid and the hydrogenation functions. This term could be characterized by the ratio of the number of accessible hydrogenating sites to the number of strong acid sites ($n_{Pt}/n_A$). The $n_{Pt}/n_A$ ratio of 0.1 wt% Pt/HY catalyst prepared by IWI and IE are 0.009 and 0.019, respectively.

In order to determine the reaction pathway of prepared catalyst, the qualitative and quantitative analysis were necessary. The major challenge in product analysis involved identification of the $n$-hexadecane isomers. As shown in Figure 4.11, the resolution of individual peaks disappeared and thus lumping of the isomers was used to simplify the kinetics analyses.

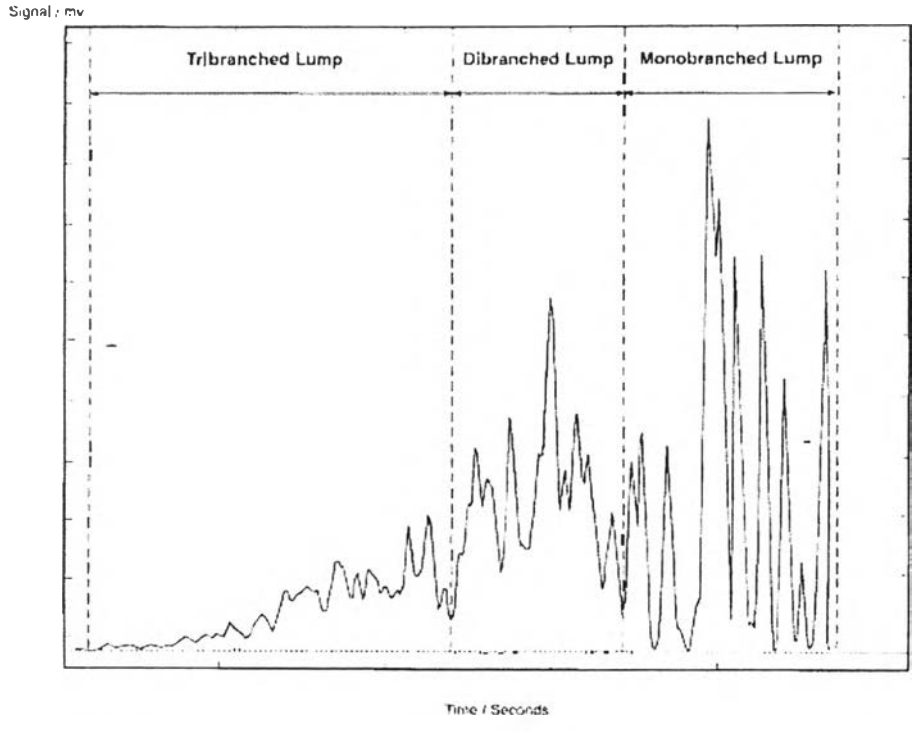


**Figure 4.11** Chromatogram of n-hexadecane and its isomerization products (Girgis and Tsao, 1996).

The products obtained from hydrocracking of *n*-hexadecane over the Pt/HY prepared by IWI and IE were lumped into four groups on the basis of changes in their relative areas at different conversion, which include with cracking product ($C_1$ to $C_{15}$), monobranced isomers, multibranced isomers (including dibranced isomers), and remaining feed.

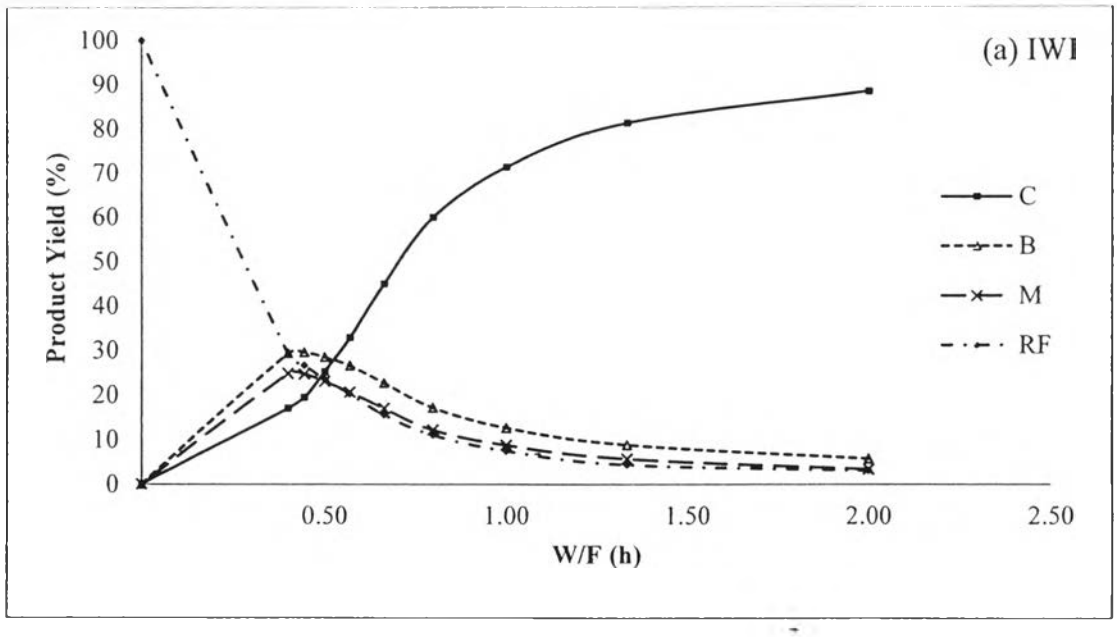


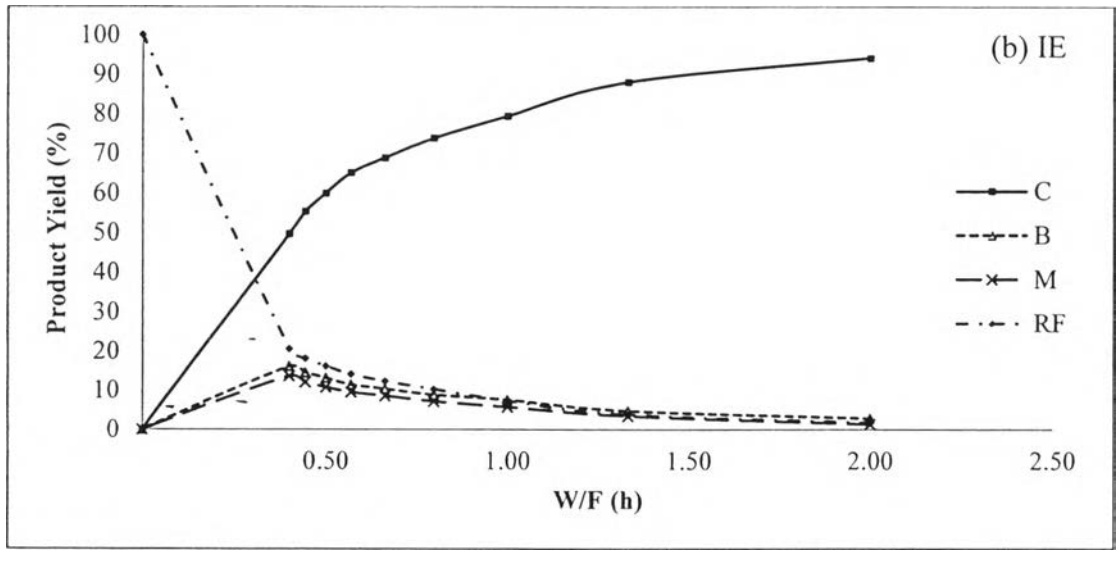


**Figure 4.12** Transformation of *n*-$C_{16}$ on Pt/HY prepared by (a) Incipient wetness impregnation and (b) Ion-exchange method: yield in monobranced isomer M, in multibranced isomer B, in cracking product C, and remaining feed RF as a function of contact time.

On both catalysts, the *n*-alkanes transformed into isomerization products (monobranced isomers and multibranced isomers) and into cracking products. Figure 4.12 shows the distributions of cracking product (C), monobranced isomers (M), multibranced isomers (B), and remaining feed (RF) obtained by hydrocracking of *n*-$C_{16}$ on the 0.1 wt% Pt/HY prepared by IWI and IE techniques as a function of contact time. Figure 4.12 (a), at the beginning, yield of cracking product was lower than yield of monobranced and multibranced isomers and cracking product yield increased with increasing of contact time until being the main product. For the IE catalyst, Figure 4.12 (b) showed that the cracking products, monobranced and multibranced were all apparent primary reaction products with a higher yield of cracking products. Then monobranced and multbranced were also converted to cracking products while the cracking products being the main products formed initially. From the product transformation curve on both catalysts, it could be proposed the same reaction pathway as shown in Scheme 4.1. However, the different reaction rates could be observed for IWI and IE catalysts. The result showed that the cracking product curve of IE catalyst has higher slope than that of IWI catalyst resulting in higher reaction rate. And this confirmed that IE catalyst gave a higher reactivity than IWI catalyst.

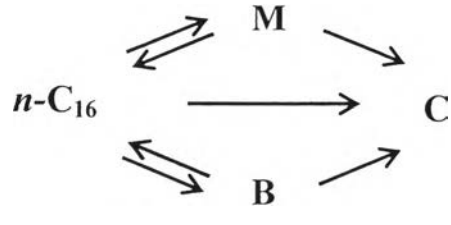


**Scheme 4.1** Proposed reaction scheme on IWI and IE catalyst

## 4.4 Characterization of Spent Catalysts

### 4.4.1 Temperature Programmed Oxidation (TPO)

Temperature programmed oxidation (TPO) technique was used to analyze the amount of the coke deposited on the spent catalysts. The TPO profiles and amounts of coke deposit on spent catalysts obtained after catalytic hydrocracking reaction of various *n*-paraffin feedstocks ($C_{15}$-$C_{18}$) over 0.1 wt% Pt/HY catalysts prepared by incipient wetness impregnation and ion-exchanged techniques are illustrated in Figure 4.13 and Table 4.7. Considering the effect of feed chain length, the results showed that the higher amount of coke was observed on longer chain length feedstock compared from spent catalyst prepared by IWI. Comparing the amount of coke deposit on spent catalyst prepared by IWI and IE, catalyst prepared by IWI had less amount of coke deposit than catalyst prepared by IE. These TPO results conformed to the total conversion value of these catalysts, the higher conversion (better cracking activity) will have more amount of coke deposit on.

**Table 4.7** Amount of carbon deposition on prepared catalyst after reaction

| Catalyst | Feedstock | Coke (wt. %) |
|---|---|---|
| Pt/HY (IWI) | *n*-$C_{15}$ | 3.35 |
| | *n*-$C_{16}$ | 3.89 |
| | *n*-$C_{17}$ | 4.78 |
| | *n*-$C_{18}$ | 5.45 |
| Pt/HY (IE) | *n*-$C_{16}$ | 4.72 |

From Figure 4.13, TPO profiles showed that the temperature required for burning coke of the spent catalyst prepared by IE was lower than catalysts prepared by IWI. This result might cause of catalyst prepared by IE has higher Pt dispersion which result of better (de)hydrogenation then it helps reducing hard coke formation. Considering spent catalysts from different feedstocks, the result showed lower coke burning temperature in shorter chain length which could be due to smaller size of coke composition that was easily removed.

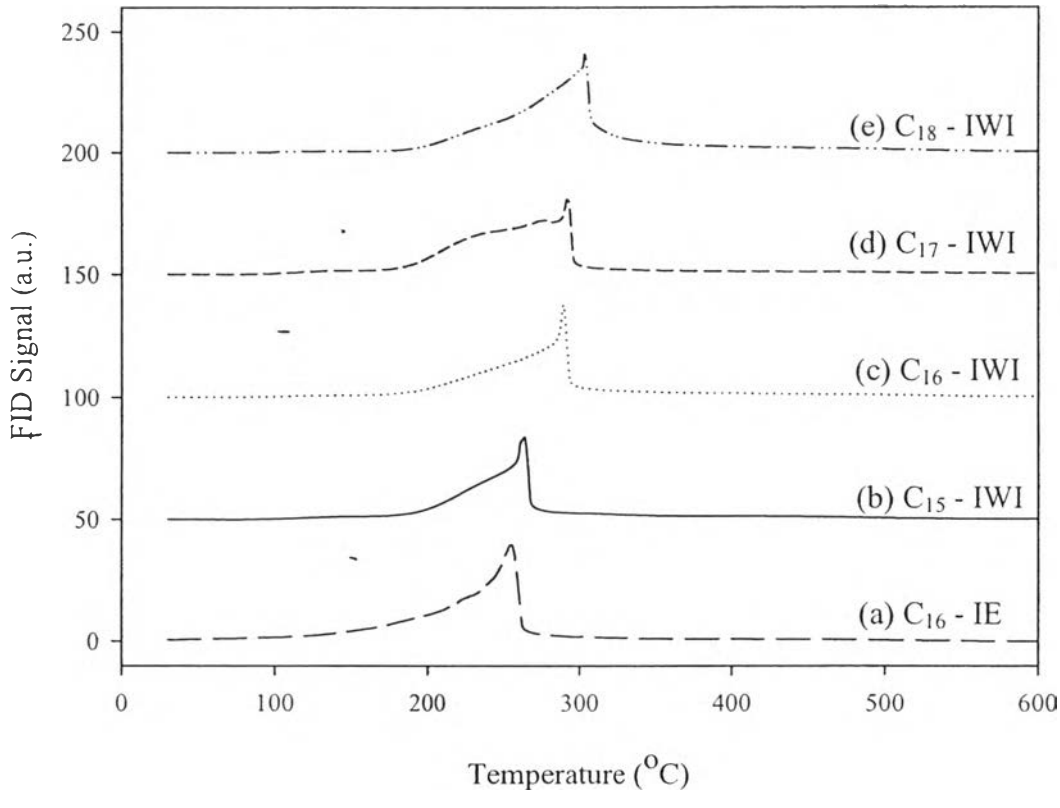


**Figure 4.13** TPO profiles of spent catalysts (a) $C_{16}$ - IE, (b) $C_{15}$ - IWI, (c) $C_{16}$ - IWI, (d) $C_{17}$ - IWI, and (e) $C_{18}$ - IWI after 6 h time on stream hydrocracking reaction.